39th AIAA/ASME/SAE/ASEE Joint Propulsion Conference and Exhibit
20-23 July 2003, Huntsville, Alabama

AIAA 2003-5162

Comparison of Discharge Plasma Parameters in a 30-cm NSTAR Type Ion Engine with and without Beam Extraction*

Daniel A. Herman†, Alec D. Gallimore‡
Plasmadynamics and Electric Propulsion Laboratory
University of Michigan
Ann Arbor, MI 48105 USA

ABSTRACT

Double Langmuir probe measurements are presented over a two-dimensional array of locations in the near Discharge Cathode Assembly (DCA) region of a 30-cm diameter ring cusp ion thruster. Discharge plasma data taken *with* and *without beam extraction* exhibit a broadening of the high on-axis electron temperature region when a beam is extracted. Electron number density and temperature contours are presented for similar discharge currents and voltages, but different cathode and main mass flow rates. Decreasing the discharge cathode flow rate tends to broaden the high on-axis electron temperature region possibly resulting from transition of the discharge cathode from spot to plume mode. Electron temperature magnitudes, 2 – 7 eV, are comparable to those measured by other researchers in electron bombardment discharge plasmas. Number density contours, with a maximum of approximately $2x10^{12}$ cm^{-3} on centerline, show very little variation over the range of operating conditions investigated. Number densities are similar to data taken by other researchers and are high enough to account for the measured erosion of the DCA in the 8200 hour wear test, as calculated by Williams, due to singly ionized xenon accelerating away from a potential hill back towards the DCA.

NOMENCLATURE

A_p	Probe surface area, m^2	P_b	Base pressure (air), Torr
A_s	Ion Collection Area, m^2	P_i	Indicated pressure (with xenon flow), Torr
e, q	Electron charge, $1.6x10^{-19}$ C	P_c	Corrected pressure (on xenon), Torr
I	Probe collected current, mA	r	Probe Electrode Radius, m
I_{sat}	Ion saturation current, A	T_{eV}	Electron temperature, eV
J_a	Acceleration grid current, mA	$V_{ck\text{-}cc}$	Keeper to cathode common voltage, V
J_b	Beam current, A	V_d	Discharge voltage, V
J_{dc}	Discharge current, A	V_g	Neutralizer to ground coupling voltage, V
J_{nk}	Neutralizer keeper current, A	V_s	Screen grid voltage, V
k	Boltzmann's constant, $1.38x10^{-23}$ J/K	V_a	Acceleration grid voltage, V
M_{Xe}	Atomic mass of xenon, kg	V_{nk}	Neutralizer keeper voltage, V
m	Electron mass, kg	λ_D	Debye Length, cm or mm
n_e,	Electron number density, cm^{-3}	ϕ	Probe bias potential, V
n_i	Ion number density, cm^{-3}	δ	Sheath thickness, cm

* Color copies available at http://www.engin.umich.edu/dept/aero/spacelab/research/conf_pub.html.
† Graduate Student, Aerospace Engineering, Member AIAA, hermo@engin.umich.edu.
‡ Associate Professor and Laboratory Director, Associate Fellow AIAA.

INTRODUCTION

Ion thrusters are high efficiency, high specific impulse (I_{sp}) propulsion systems proposed as the primary propulsion source for a variety of missions. In some cases ion thruster technology has enabled new missions that had not been feasible using liquid propellant rocket technology. NASA's Dawn mission, propelled by three 30-cm ion thrusters, will study two minor planets, Ceres and Vesta, that reside in the vast asteroid belt between Mars and Jupiter.[1] The NASA Solar Electric Propulsion Technology Applications Readiness (NSTAR) 30-cm ion thruster was the first ion engine to be used for primary spacecraft propulsion, validating ion thruster technology, and demonstrating operation for over three times its intended lifetime.[2] Nevertheless, efforts to further increase engine lifetime continue.

A potential failure mechanism for an ion engine is erosion of the discharge cathode.[3] A cathode keeper was added, as an engineering solution, in order to mitigate cathode erosion on NSTAR.[4] Adding the keeper reduced the cathode erosion rate to acceptable levels and until recently was thought to have solved the Discharge Cathode Assembly (DCA) erosion issue. An Extended Life Test (ELT) of the NSTAR flight spare thruster, conducted at the Jet Propulsion Laboratory (JPL), revealed extensive keeper erosion that has yet to be fully explained.[5-7] Although the engine continues to operate after 28,000 hours of operation (over 200 kg of xenon processed)[7], there exists a clear need to understand the cause of DCA erosion, how engine operating conditions affect DCA erosion, and how to reduce DCA erosion thereby extending engine lifetime.

Laser Induced Fluorescence (LIF) measurements done by Williams have suggested the existence of a potential hill downstream of the DCA as a possible cause of DCA erosion.[8-10] Direct measurement of plasma properties, such as electron temperature, electron number density, and plasma potential would validate or rule out the possibility that a potential hill causes discharge cathode erosion by accelerating a portion of the ions away from the hill towards the DCA.

Mapping the internal plasma structure of the 30-cm ion engine, downstream of the DCA, as a function of engine operating condition is essential to understanding the cause of DCA erosion.

30-CM ION THRUSTER

Background

The Functional Model Thruster (FMT) preceded the NSTAR Engineering Model Thruster (EMT) and the NSTAR Flight Thruster. The principal difference in the construction of the FMT from the EMT is the anode material. The FMT anode is aluminum while the EMT anode is spun aluminum and titanium. The second of two FMTs, FMT-2, was modified at the NASA Glenn Research Center (GRC) by Williams to allow optical access to the discharge chamber for LIF measurements.[8] Six slots were cut into FMT-2: three slots in the anode wall and three slots in the plasma shield.

Three quartz windows covered the rectangular slots cut into the FMT-2 anode wall during LIF measurements. These three slots, each 10.2 cm by 3.2 cm, replaced roughly twenty percent of the anode surface. The side slots of the plasma shield and anode are shown in Fig. 1.

The magnetic field, DCA, and geometry of the discharge chamber are identical to those of the EMT-1.[8] For a more complete comparison between FMT-2 and EMT-1 see Reference 8. The thruster has been operated over the entire NSTAR power throttling range at GRC and at the Plasmadynamics and Electric Propulsion Laboratory (PEPL) illustrating comparable performance to the EMTs and flight thrusters. Williams has shown that these modifications have not altered the discharge chamber magnetic field, the ion production efficiency, or the overall thruster performance.[8]

Discharge Plasma Containment Mechanism

The side anode quartz window is replaced by a Discharge Plasma Containment Mechanism (DPCM) allowing electrostatic probe access inside the anode. The first design iteration consisted of 44-gauge stainless steel foil held between stainless steel guides that force the foil to curl as the probe moved downstream of the DCA.

A 99.8% pure alumina tube extended from the plasma shield into the anode, isolating the probe from both anode and ground while maintaining isolation between anode and ground. This design proved flawed due to the formation of rips or tears in the foil after multiple axial cycles. A more complete description of the original design can be found in Reference 11.

The new design, shown in Figures 2 – 4, replaces the 44-gauge curling sheet with a series of overlapping 38-guage slotted stainless steel sheets. Repeatable axial movement of the probe is possible without the formation of rips. Discharge plasma containment is maintained and visually monitored during thruster operation via an adjacent vacuum-rated camera. Any visible hole or tear formation, while extracting a beam, leads to a surge of discharge plasma towards the hole as the high-voltage plasma escapes to ground. Repeated recycles of the engine occur when this happens that often overload the isolation amplifiers in the double probe circuit.

The ability to retract and extend the translating alumina tube at various axial locations minimizes protrusion of material into the discharge chamber. The alumina tube extends approximately 2 cm inside of the discharge chamber wall at all axial locations. The alumina tube is mounted onto a New England Affiliated Technologies (NEAT) RMS-800 single axis ball screw table controlled via computer. The table has a lead screw accuracy of 80 μm and a range of motion of 20 cm.

To minimize the likelihood of contaminating and perturbing the discharge plasma, the probe is recessed in the low-density interior of the alumina tube when not in use. A rectangular aluminum plate eliminates the line of sight of background particles to the anode.

APPARATUS AND PROCEDURE

Vacuum Facility

All experiments are performed in the 6 m by 9 m Large Vacuum Test Facility (LVTF) at PEPL. Four of the seven CVI Model TM-1200 Re-Entrant Cryopumps are used for these experiments, which provide a combined pumping speed of 140,000 l/s on xenon with a base pressure of ~3×10^{-7} Torr. Chamber pressure is recorded using two hot-cathode ionization gauges. The pressure reported is an average of the two corrected readings. A complete neutral pressure map of the LVTF has shown that the average pressure is a conservative measure of the tank pressure in this facility.[12] Pressure measurements from each gauge are corrected for xenon using the known base pressure on air and a correction factor of 2.87 for xenon according to,[13,14]

$$P_c = \frac{P_i - P_b}{2.87} + P_b \,. \qquad (1)$$

A dedicated propellant feed system, consisting of three Edwards mass flow controllers provided by NASA GRC, control the xenon flow rate to the thruster. The flow rates are periodically calibrated using a known volume technique.

A 2 m by 2.5 m louvered graphite panel beam dump is positioned approximately 4 m downstream of the FMT-2 to reduce back sputtering. The thruster is operated at PEPL using a modified Skit-Pac provided by NASA GRC.

Axial Movement

The FMT-2 is mounted on a custom built, two-axis positioning system consisting of two NEAT translational stages. The upper axis maintains a constant radial distance between the thruster and the High-speed Axial Reciprocating Probe (HARP) positioning system. The lower axis controls the engine axial location with respect to the probe to an absolute position accuracy of 0.15 mm. The electrostatic probe is radially positioned inside the discharge chamber using the HARP. The HARP system is fixed to the chamber wall. When actuated, the probe extends to the thruster centerline then returns to the starting location recessed inside the translating alumina tube. The RMS-800 NEAT table retracts and extends the translating alumina tube as the axial location changed.

High-speed Axial Reciprocating Probe (HARP)

A linear motor assembly provides highly accurate direct linear motion of the probe with minimal discharge chamber residence times. The HARP system is a three-phase brushless dc servo motor consisting of a linear "U"-shaped magnet track and a "T"-shaped coil moving on a set of linear tracks.

The linear encoder provides positioning resolution to 5 μm.[15] A Pacific Scientific SC950 digital, brushless servo drive controls the motor. A PC monitors and controls the servo drive via serial cable. The entire table is enclosed in a stainless steel shroud with a graphite outer skin. Residence times of the probe inside the discharge chamber are kept under one second to minimize probe heating and discharge plasma perturbation. Additional information of the HARP system can be found in References 15 and 16.

FMT-2 Operation

Since the current investigation focuses on near DCA plasma phenomena, the primary thruster operating parameters are the discharge current and voltage. For each operating condition, *without beam extraction*, the discharge current is set to the desired value corresponding to the discharge current in the NASA Throttling table (TH Level). The main anode flow rate and discharge cathode flow rate are adjusted so the discharge voltage matches the respective value for the desired NASA TH Level. The discharge only operating conditions, *i.e. without beam extraction*, of the FMT-2 are referred to as Discharge Levels (DL).

The procedure for operating the FMT-2 *with beam extraction* is to slowly throttle up the discharge current to match the desired NASA TH Level discharge current. The main and discharge flow rates are adjusted until both the discharge cathode voltage and beam current match those recorded in the NASA throttling table. The data taken *with beam extraction* are referred to as Thruster Operating Conditions (TOC Levels). Referring to them as Throttling Levels (TH) would be erroneous because not all of the thruster operating parameters are matched. Tables 1 – 3 report the complete listing of the discharge parameters and thruster telemetry for the operating conditions investigated.

The typical data collection time was one hour for each operating condition. In order to maintain discharge voltage and beam current, the cathode and main flow rates were sometimes adjusted slightly during data collection. The maximum and minimum flow rates during data collection are recorded.

ELECTROSTATIC PROBE

Probe Type

Several factors are taken into consideration when designing the electrostatic probe, the first being the type of probe. Unlike the single Langmuir probe, the double probe floats as a whole, which both minimizes discharge plasma perturbation and allows the probe electrodes to follow discharge plasma oscillations.[17] The symmetric geometry of the double probe about the discharge cathode orifice makes it more appealing than using a triple probe. A symmetric double probe is selected over an asymmetric double probe because the simplicity in data analysis outweighed the benefits gained by sampling more of the electron energy distribution. A major drawback of the double probe is that there is no distinction between primary and Maxwellian electron populations.

Double Probe Hardware

Probes always perturb their surroundings, however the extent of the perturbation is minimized by physically making the probe as small as possible. This bodes well with the need to maintain spatial resolution when making measurements. To minimize the plasma losses to the probe, which would unduly perturb the discharge plasma, the probe size is minimized while maintaining a measurable current based on predicted plasma parameters.

The electrodes of the double probe are sized such that, for the expected electron temperature (2 – 11 eV)[18,19] and number densities ($1x10^{10}$ – $1x10^{12}$ cm^{-3}),[18,20] the probe operates in the thin sheath regime. The number densities are expected to have a maximum on cathode centerline and decrease by over two orders of magnitude with increasing radial distance from centerline driving an ever-increasing Debye length. The relationship of the Debye length to electron number density and temperature is illustrated in Equation 2:[29-30]

$$l_D = 743\sqrt{\frac{T_{eV}}{n_e}}\,. \qquad (2)$$

In the thin sheath regime, the flux of particles entering the sheath can be calculated without considering the details about the orbits of these particles in the sheath.[17,21-23]

In this case, the collection area of the electrode is approximated as the area of the electrode, which is justified for a large ratio of probe radius to Debye length, λ_D.[17,21,23] However, the rapid growth in the Debye length with increasing radial distance from cathode centerline dictates that, at some radial location inside the anode, the thin sheath criterion may not strictly apply. Accordingly, the thin sheath calculation is used until the Debye length is equal to the electrode radius.

A large length to diameter ratio minimizes end effects. A conservative gap distance – the distance between the probe electrodes – maintains a minimum factor of three times the sum of the two electrode sheaths (*i.e.*, 3 x 2 x $5\lambda_D$) to avoid overlapping.

Three similar double probes were used during the test due to breaking of probes during setup and testing. All probes were slight variations on the basic double probe design used, shown in Fig. 5. Two 0.381 mm diameter cylindrical tungsten electrodes, with 4 mm exposed length, are held inside two double bore pieces of 99.8% pure alumina epoxied to one larger double bore piece of 99.8% pure alumina. The total length of the tungsten and alumina is approximately 46 cm (18 inches). The "double tier" design reduces the amount of blockage mass that is inserted into the discharge cathode plume.

Double Probe Electronics

During probe insertion into the discharge plasma, the floating potential rapidly increases as high as 1100 V, causing difficulty for most electronics. Significant errors in the measured current can occur due to any appreciable stray capacitance in the circuit. As such, careful attention is paid to minimizing stray capacitance in the circuit design including the use of batteries to supply the bias voltage.[16] The battery supply consists of two series groups of four 67.5-volt zinc-manganese dioxide batteries connected in parallel. The batteries are capable of outputting 135 V at 100 mA. A potentiometer is attached to the battery output to adjust the electrode bias voltage.

The double probe circuit, previously used to make similar measurements inside the discharge channel of a Hall Thruster[16], is built around two Analog Devices AD210 isolation amplifiers. These amplifiers are capable of handling up to 2500 volts of common mode voltage and provide an input impedance of $1x10^{12}$ Ω. The low impedance output (1 Ω maximum) is connected to a Tektronix TDS 3034B digital oscilloscope that, when triggered off the probe position, records the data and saves it to a computer. Figure 6 illustrates the double probe circuit. The outputs of the isolation amplifiers are calibrated with known currents and bias voltages over their entire operating ranges.

DATA ACQUISITION

To reduce data collection time, the three NEAT tables are controlled by one LabVIEW code that allows multiple input positions, the ability to wait at a given location, the ability to trigger the HARP, and record the data from the oscilloscope after each sweep. The automation increases the spatial resolution for a given amount of time.

The two NEAT translational stages and NEAT RMS-800 stage are controlled via GPIB connections. A LabVIEW code steps through the full axial range of motion (approximately 4 cm) in 1.6 mm increments. For each axial step, the program retracts the alumina translating tube radially, sweeps the probe radially through the discharge plasma, and dwells for the amount of time required for the HARP sweep of the probe. After all axial locations are interrogated, the computer returns the FMT-2 to the zero axial position located 2 mm downstream of the DCA exit plane. Bias voltages are set manually using a potentiometer and the battery supply. The probe is then swept through all spatial locations. The bias voltage is then manually changed and the process repeats until the 31 bias voltages are investigated.

The HARP is controlled by a separate computer using serial connections. A Tektronix TDS 3034B oscilloscope triggers off of the HARP position and records all data. The oscilloscope records probe position, probe collected current, probe bias voltage, and the discharge current (from a Hall sensor) as a function of time during probe insertion. From the oscilloscope raw data, the discharge current, probe collected current, and probe bias voltage are calculated as a function of probe position. The resulting data are reassembled to obtain the current-voltage characteristic (I-V curve) of the double probe at each spatial location in the radial sweep.

Only data taken on the "in sweep" of the probe are analyzed as "out sweep" data are more likely to be affected by probe perturbation. Figure 7 illustrates probe insertion into the discharge plasma. Figure 8 illustrates the two-dimensional data collection domain. The discharge current perturbation induced by the double probe is measured using a Hall Probe, in conjunction with the Tektronix TDS 3034B oscilloscope. Discharge current perturbation is approximately 5 - 10%.

DATA ANALYSIS

The scientific graphing package Igor is used to analyze the data. The data are read into Igor, which reassembles the data into individual characteristics at each spatial location in the two-dimensional grid. The individual double probe characteristics are analyzed assuming an infinite, quasi-neutral, and quiescent plasma. The electron and ion mean free paths are much larger than the probe dimensions indicating a collisionless analysis. Particles are assumed to be collected without reflection or reaction inside the electrode collection area.

The presence of a magnetic field has a negligible effect on the probe measurements. The double probe analysis infers number density from the ion saturation current and therefore is unaffected by the reduction in electron saturation current caused by the presence of a magnetic field. The magnetic field can also lead to electron energy distribution function (EEDF) anisotropy. Passoth[24] determined that EEDF anisotropy depends upon the ratio B/p_o, where p_o is the pressure in the containment vessel (in this case the discharge chamber). It has been shown experimentally that EEDF anisotropy is negligible for $B/p_o \leq 2.5 \times 10^6$ G/Torr.[25] In the FMT-2, B has a maximum (downstream of the DCA) of 107 G and the pressure in the discharge chamber is estimated to be $\sim 10^{-4}$ Torr. The value of B/p_o for the worst case is 1×10^6, therefore no substantial anisotropy in the EEDF is expected.

Post test inspection of the raw data revealed asymmetric I-V curves. The asymmetry is most extreme closest to the DCA, decreasing with increasing axial distance from the DCA. The asymmetry is larger than can be accounted for by differing electrode lengths. The most probable cause is electrode to orifice misalignment occurring during pumpdown. The HARP, and thus the electrostatic probe, is mounted to the wall of the chamber, while the engine rests on a platform inside the vacuum facility. During pumpdown the walls of the chamber compress resulting in a shift of the probe tip. A vertical shift of one millimeter would result in one electrode lying directly in front of the discharge cathode plume. The disappearance of the asymmetry far from the plume supports the misalignment theory. Mounting both the engine and the HARP on a common structure, independent of the chamber wall, would eliminate this problem.

To account for the misalignment shift, the electrode collected current and bias voltage data corresponding to the larger collected current, *i.e.* the electrode in the discharge cathode plume, is mirrored and the resulting I-V curve is used for the fit. Each I-V characteristic is fitted with the theoretical hyperbolic tangent curve for a symmetric cylindrical double probe, Equation 3, incorporating the Levenberg-Marquardt fit method.[17,26-28]

$$I = I_{sat} \cdot \tanh\left(\frac{f}{2T_{eV}}\right) + A_1 \cdot f + A_2 \qquad (3)$$

In Equation 3, the parameter A_1 accounts for sheath expansion in the ion saturation region and A_2 accounts for any offset current due to stray capacitance. Figures 9 – 11 illustrate representative I-V traces and their corresponding curve fits. Electron temperature can be determined immediately from the fit parameters. Using the Bohm approximation[17,29,30] for ion velocity, the ion number density is calculated according to Equation 4:

$$n_i = \frac{I_{sat}}{A_s (q)^{3/2}} \sqrt{\frac{M_{Xe}}{T_{eV}}}\,. \qquad (4)$$

In this equation, A_s is initially considered to be the electrode surface area. The true collection area depends upon the thickness of the sheath surrounding the probe. Knowledge of the number density and electron temperature allows the Debye length to be calculated according to Equation 2 (Figs. 12 and 13). Assuming quasi-neutrality $n_e \approx n_i$ (in cm^{-3}) readily gives λ_D (cm).

The sheath is calculated according to Equation 5:[23,32]

$$d = 1.02\,l_D\left[\left(\frac{1}{2}\ln\left(\frac{m}{M_{Xe}}\right)\right)^{1/2} - \frac{1}{\sqrt{2}}\right]^{1/2}\left[\left(\frac{1}{2}\ln\left(\frac{m}{M_{Xe}}\right)\right)^{1/2} + \sqrt{2}\right] \quad (5)$$

and the sheath area follows from Equation 6:[22]

$$A_s = A_p\left(1 + \frac{d}{r}\right). \quad (6)$$

New plasma parameters are calculated from this new collection area. This process attempts to take into account the departure from the thin sheath regime.

Typical estimates for the error in electron temperature and electron number density are 20% and 50%, respectively.[22] For double probe measurements the electron temperature is evaluated according to Equation 7.[17] Errors in estimating both the slope of the characteristic at zero bias and the ion saturation current lead to errors in electron temperature.

$$T_{eV} = \frac{e}{k}\left(\frac{I_{sat}}{2\,dI/df\big|_{f=0}}\right) \quad (7)$$

RESULTS AND DISCUSSION

No data taken *with beam extraction* for TOC 12 – corresponding to TH Level 12 – are presented because an incomplete data set was taken.

Electron Temperature Contours

Figures 14 – 27 illustrate the calculated electron temperatures. Each contour contains an on-axis maximum region, the exception being electron temperature data taken Nov. 2002. Comparison of the electron temperature contours shows that as the cathode flow rate is decreased the high electron temperature region tends to broaden and/or increase in magnitude. This may be due to starving of the cathode resulting in a shift from spot to plume mode.[19] As the cathode flow rate is decreased, ion flux to the keeper and discharge plasma decreases and becomes insufficient to neutralize space charge. The space charge limitations only allow high-energy electrons to escape.[19] The result is an increase in the mean electron temperature of the emitted plasma from the cathode.

Electron temperature contours of data taken *with beam extraction* illustrate a wider, high electron temperature area on DCA centerline when compared to data taken *without beam extraction* of comparable cathode flow rates (compare Figure 18 with Figure 19 and Figure 25 with Figure 27 for two examples of this trend).

It is difficult to compare higher cathode flow rate contours *with beam extraction* to lower cathode flow rate *without beam extraction* contours. In these cases, a combination of the two effects is present and, depending upon the magnitude of the cathode flow rate difference, may result in either an increase (broadening) or decrease (narrowing) of the high temperature region.

Electron temperatures range from 2 – 5 eV over most of the locations and operating conditions investigated. Larger electron temperatures, as high as 7 eV, were measured near the DCA on-axis for low cathode flow rates and high discharge currents.

Noise in electron temperature contours is evident. As previously stated, the double probe electron temperature calculation is proportional to the ion saturation current divided by the slope of the I-V characteristic evaluated at zero. As a result, errors in calculating both the ion saturation current and slope at the zero location lead to large variations in electron temperature measurements. Single Langmuir probe measurements calculate electron temperature based only on the slope of the I-V curve in the electron-retarding region and therefore may yield smoother contours.

Electron temperature measurements, taken by Williams on a 6.4 mm diameter hollow cathode (similar to the FMT-2 and NSTAR cathodes) in a cylindrical anode with a xenon cathode flow rate of 4 sccm and cathode emission current of 6 A, measured electron temperatures of 2 – 4 eV in spot mode and 2 – 6 eV in plume mode.[8] Though this is consistent with the presented data, Williams' on-axis electron temperatures increased with axial distance from the cathode. The increasing electron temperature may result from the removal of the lower temperature population of electrons by the anode.[8]

The anode used in Williams' experiment consisted of a 6.35 cm diameter cylinder without a magnetic field. The close proximity of the anode to the cathode may account for the increase in electron temperature with increasing axial distance.

Beattie and Matossian computed a spatially varying Maxwellian electron temperature profile whose maximum lies along the thruster centerline.[18] Although they studied a mercury ion thruster, one could draw the conclusion that while the electron temperature magnitudes may differ, the overall trends should be similar. Their computational results follow the trends observed in the current investigation and do not predict an increase in electron temperature with increasing axial distance from the keeper as has been measured by other researchers.

Number Density Contours

The number density measurements are illustrated in Figures 28 – 41. There is little variation between the number density contours over the range of operating conditions investigated. The number density near the DCA does not appear to be sensitive to beam extraction characteristics. In fact, the number density profiles near the DCA *with* and *without beam extraction* are essentially identical. The structure of each number density plot is similar and intuitive. There is an on-axis maximum near the DCA (in its plume) that decreases gradually in the downstream (axial) direction. A more extreme density gradient exists in the radial direction particularly at axial locations near the DCA. The number density falls off by at least an order of magnitude only 10 mm radially from the centerline. As the discharge current is increased, the magnitude of the number density plume tends to increase slightly. All number densities measured in the 2D domain fall within the expected range with values from $1x10^{10}$ – $2.4x10^{12}$ cm^{-3}. The measured number densities are within the range required to cause DCA erosion from singly-ionized xenon that is consistent with the 8200 hour wear test results, as stipulated by Williams.[3,8]

Williams' Langmuir probe data exhibit a drop in number density with increasing axial distance from the DCA along centerline consistent with the current measurements (by an order of magnitude after 4 cm). In addition, his maximum number density was measured at the nearest axial location (5 mm) and was $2x10^{12}$ cm^{-3}.[8,33]

Foster and Patterson have taken high current hollow cathode measurements on a 12.7 mm hollow cathode inside an NSTAR type discharge chamber. Radial measurements taken 3 mm downstream of the keeper plate report a maximum number density of approximately $2x10^{12}$ cm^{-3} on-axis with steep radial gradients, similar to the present data. Their results also indicate an increase in number density with increasing discharge current consistent with the current measurements.[20]

ERROR ANALYSIS

Traditional estimates of the error in electrostatic probe measurements are 50% for electron number density and 20% for electron temperature.[22] While these errors are large, the relative error between two measurements using identical setups is not believed to be as large. Noise in measured electron temperatures is evident due to the combination of errors in estimating both the slope at the zero bias location and the ion saturation current.

The disparity in electron temperature structure between data taken in Nov. 2002 and all other contours, specifically the off-axis maximum, needs to be addressed. Due to the time between measurements, different probes, and different alignment errors, it is difficult to compare the data taken in Nov. 2002 with the current data. The largest difference between these measurements, and likely the cause of the off-axis electron temperature maximum, is that the Nov. 2002 probe contained an additional floating stainless steel sleeve, 15 cm in length over the probe alumina tube, extending up to 4.4 cm from the double probe electrodes. The introduction of a conducting piece of metal extending roughly from the DCA region to the anode wall could short out the plasma.

The electron temperature contour of the data taken in Nov. 2002 (Figure 17) shows a similar structure to DL 4B (Figure 16) except in the region from approximately 20 mm radial to DCA axis. Over the 0 – 20 mm radial locations the conducting sleeve might have been close enough to the high density region to cause a macroscopic disturbance to the plume thereby removing the high-energy electrons from being collected by the electrodes.

Figures 12 and 13 are the calculated Debye length contours for the worst case and a typical case, respectively. The largest Debye lengths occur close to the anode wall and were as high as 0.11 mm, which is smaller than the 0.191 mm electrode radius. Typical Debye lengths over most of the spatial domain are 0.05 – 0.07 mm implying that, over the domain of interest, the thin sheath assumption is justified.[17,21,23]

CONCLUSIONS

Electron temperature and number density measurements inside the discharge chamber of a 30-cm ring-cusp ion thruster are presented for operating conditions *with* and *without beam extraction*. Electron temperature magnitudes, 2 – 7 eV, are comparable to those measured by other researchers in electron bombardment discharge plasmas. The extraction of a beam results in a broadening of the high on-axis electron temperature region, but no appreciable effect on number density when compared to similar cathode flow data *without beam extraction*. Decreasing the cathode flow rate has a similar effect of increasing the magnitude of and/or broadening the high electron temperature region. Number density contours, with a maximum of approximately $2x10^{12}$ cm^{-3} on centerline, show very little variation over the range of operating conditions investigated. Number densities agree with data taken by other researchers and are high enough to account for the measured erosion of the DCA in the 8200 hour wear test from singly-ionized xenon.

ACKNOWLEDGEMENTS

We would like to thank Dr. James Haas for his assistance. We would like to thank the entire research group at PEPL who have been instrumental in this investigation.

We would also like to thank Mr. Michael Patterson of the NASA Glenn Research Center (GRC) for the financial support of this research through research grant NAG3-2216 and for use of government equipment. We would like to acknowledge Dr. Matthew Domonkos (grant monitor), Dr. John Foster, and Dr. George Williams who have been principal contacts at NASA GRC. Mr. Daniel Herman is supported through a Department of Defense NDSEG fellowship

REFERENCES

[1] http://solarsystem.nasa.gov/missions/astmissns/ast-dawn.html

[2] http://nmp.jpl.nasa.gov/ds1/gen/mission.html

[3] Polk, J. E., et al., "An Overview of the Results from an 8200 Hour Wear Test of the NSTAR Ion Thruster," AIAA Paper # 99-2446, *35th AIAA / ASME / SAE / ASEE Joint Propulsion Conference*, Los Angeles, CA, June 1999.

[4] Williams, G. J., et al., "Characterization of FMT-2 Discharge Cathode Plume," IEPC Paper #99-104, *26th International Electric Propulsion Conference*, Ketakiushu, Japan, Oct. 1999.

[5] Anderson, J. R., et al, "Performance Characteristics of the NSTAR Ion Thruster During and On-Going Long Duration Ground Test," IEEE Paper No. 8.0303, *IEEE Aerospace Conference*, Big Sky, MT, Mar. 2000.

[6] Domonkos, M. T., Foster, J. E., Patterson, M. J., "Investigation of Keeper Erosion in the NSTAR Ion Thruster," IEPC Paper No. 01-308, *27th International Electric Propulsion Conference*, Pasadena, CA, Oct. 2001.

[7] Sengupta, A., Brophy, J. R., and Goodfellow, K. D., "Wear Characteristic from the Extended Life Test of the DS1 Flight Spare Ion Thruster," *28th International Electric Propulsion Conference*, Toulouse, France, March 17-21, 2003.

[8] Williams, G. J., *The Use of Laser-Induced Fluorescence to Characterize Discharge Cathode Erosion in a 30 cm Ring-Cusp Ion Thruster*, Ph.D. Dissertation, Univ. of MI, 2000.

[9] Kameyama, I., and P. J. Wilbur, "Potential-Hill Model of High-Energy Ion Production Near High-Current Hollow Cathodes," ISTS-98-Aa2-17, 21st International Symposium on Space Technology and Science, (May, 1998).

[10] Hayakawa, Y., Miyazaki, K., Kitamura, S., "Measurements of Electron Energy Distributions in a 14 cm Diameter Ring Cusp Ion Thruster," *Journal of*

propulsion and Power, Vol. 8, pp. 118 – 126, Jan – Feb, 1992.

[11] Herman, D. A., McFarlane, D. S., and Gallimore, A. D., "Discharge Plasma Parameters of a 30-cm Ion Thruster Measured without Beam Extraction using a High-Speed Probe Positioning System," IEPC-03-0069, *28th International Electric Propulsion Conference*, Toulouse, France, March 17-21, 2003.

[12] Walker, M. L. R., Gallimore, A. D., "Pressure Map of a Facility as a Function of Flow Rate to Study Facility Effects," *AIAA-2002-3815, 38th Joint Propulsion Conference*, Indianapolis, Indiana, July 7-10, 2002.

[13] Hofer, R. R., Peterson, P. Y., Gallimore, A. D., "Characterizing Vacuum Facility Backpressure Effects on the Performance of a Hall Thruster," IEPC Paper No. 01-045, *27th International Electric Propulsion Conference*, Pasadena, CA, Oct. 2001.

[14] Dushman, S., *Scientific Foundations of Vacuum Technique*, Vol. 4, Wiley, N.Y., 1958.

[15] Haas, J. W., et al, "Development of a High-Speed, Reciprocating Electrostatic Probe System for Hall Thruster Interrogation," *Review of Scientific Instruments*. Vol. 71, No. 11, pp. 4131-4138, Nov. 2000.

[16] Haas, J. W., *Low-Perturbation Interrogation of the Internal and Near-Field Plasma Structure of a Hall Thruster using a High-Speed Probe Positioning System*, Ph.D. Dissertation, University of Michigan, 2001.

[17] Mott-Smith, H., and Langmuir, I. *Physics Review*, Vol. 28, 727, 1926.

[18] Beattie, J. R., and Matossian, J. N., *Mercury Ion Thruster Technology* Final Report, NASA CR-174974, Hughes Research Labs. Feb. 1983 – Oct. 1984.

[19] Domonkos, M. T., *Evaluation of Low-Current Orificed Hollow Cathode*, Ph.D. Dissertation, University of Michigan, 1999.

[20] Foster, J. E., and Patterson, M. J., "Plasma Emission Characteristics from a High Current Hollow Cathode in an Ion Thruster Discharge Chamber," *AIAA-2002-4102, 38th Joint Propulsion Conference*, Indianapolis, Indiana, July 7-10, 2002.

[21] Hershkowitz, N., "How Langmuir Probes Work," *Plasma Diagnostics*. Nuclear Engineering and Engineering Physics Department, Univ. of Wisconsin-Madison, 1989.

[22] Hutchinson, I. H., *Principles of Plasma Diagnostics*, Cambridge University Press, New York, N.Y., 1987.

[23] Schott, L. *Plasma Diagnostics: Ch. 11 Electrical Probes*, American Elsevier Publishing Co, New York, N.Y., 1968.

[24] Passoth, E., et al, "An experimental study of plasma density determination by a cylindrical Langmuir probe at different pressures and magnetic fields in a cylindrical magnetron discharge in heavy rare gases," *Journal of Physics D.*, Vol. 30, No. 12, June 1997, p. 1763-77.

[25] Aikawa, H., "The Measurement of the Anisotropy of Electron Distribution Function of a Magnetized Plasma," *Journal of the Physical Society of Japan*, Vol. 40, No. 6, June 1976.

[26] Johnson, E. O., and Malter, L., "A Floating Double Probe Method for Measurements in Gas Discharges," *Physics Review*, Vol. 80, No. 1, pp. 58 - 68, Oct., 1950.

[27] Boedo, et al, "Fast Scanning Probe for Tokamak Plasmas," *Review of Scientific Instruments*, Vol.69,#7, pp. 2663-70, July, 1998.

[28] Smith, B. A, and Overzet, L., J., "Improvements to the Floating Double Probe for Time-resolved Measurements in Pulsed RF Plasmas," *Review of Scientific Instruments*, Vol. 69, No. 3, pp. 1372 – 1377, March, 1998.

[29] Chen, F.F. *Introduction to Plasma Physics and Controlled Fusion: Vol. 1 Plasma Physics*, Plenum Press, New York, N.Y., 1984.

[30] Chen, F. F., *Plasma Diagnostic Techniques: Ch. 4 Electric Probes*, Academic Press, New York, N.Y., 1965.

[31] *NRL Plasma Formulary*, NRL/PU/6790--00-426, Naval Research Laboratory, Washington, D.C., 2000.

[32] Ruzic, D. D., *Electric Probes for Low Temperature Plasmas*, American Vacuum Society Educational Committee, New York, N.Y., 1994.

[33] Williams, G. J., et al., "Near-Field Investigation of Ions Emitted from a Hollow Cathode Assembly Operating at Low-Power," AIAA-98-3658, *34th Joint Propulsion conference*, July, 1998.

Table 1 – FMT-2 discharge operating parameters for Thruster Operating Conditions *(with beam extraction)* and Discharge Levels *(without* beam extraction) roughly corresponding to the same discharge current and voltage as NASA Throttling Levels.

Level	V_{dc} [V]		J_{dc} [A]	Main flow rate [sccm]		Disch. Cath. flow rate [sccm]		Pressure [Torr]
	min	max		min	max	min	max	corrected
TOC 4	25.50	25.70	6.05	8.5	8.9	4.92	5.50	2.5E-06
DL 4A	25.51	25.71	6.05	11.6	12.6	4.07	4.07	2.3E-06
DL 4B	25.36	25.46	6.05	19.2	19.8	2.54	2.54	3.1E-06
TOC 8	25.00	25.20	8.24	15.2	15.5	3.99	4.05	2.5E-06
DL 8A	25.00	25.20	8.24	15.6	17.0	3.10	3.64	2.7E-06
DL 8B	25.10	25.20	8.24	15.0	16.6	2.54	2.54	2.5E-06
DL 8C	25.10	25.20	8.24	20.8	22.2	2.73	2.83	3.3E-06
DL 8D	25.00	25.20	8.24	22.3	23.7	3.17	3.17	3.5E-06
TOC 12	25.30	25.50	10.87	21.1	21.4	3.26	3.30	3.9E-06
DL 12A	25.30	25.50	10.87	14.7	17.2	1.93	2.52	2.8E-06
DL 12C	25.40	25.50	10.87	14.0	18.4	2.89	2.89	2.5E-06
TOC 15	25.04	25.24	13.13	24.9	25.3	2.92	2.99	4.4E-06
DL 15A	25.00	25.30	13.13	11.4	11.4	2.00	2.34	2.0E-06
DL 15C	25.00	25.20	13.13	8.4	8.4	3.38	3.56	1.7E-06

Table 2 – FMT-2 discharge operating parameters highlighting the data taken, and NASA throttling level corresponding to, a discharge current of 6.05 A and a discharge voltage of ~25.6 V.

Level	V_{dc} [V]		J_{dc} [A]	Main Flowrate [sccm]		Disch. Cath. flow rate [sccm]		Pressure [Torr]
	min	max		min	max	min	max	corrected
Nov-02	25.40	25.80	6.05	8.1		2.29		1.6E-06
TOC 4	25.50	25.70	6.05	8.5	8.9	4.92	5.50	2.5E-06
DL 4A	25.51	25.71	6.05	11.6	12.6	4.07	4.07	2.3E-06
DL 4B	25.36	25.46	6.05	19.2	19.8	2.54	2.54	3.1E-06
TH 4	25.61		6.05	8.30		2.47		-

Table 3 – Nominal Thruster Operating Conditions (TOC Levels) and reference NASA Throttling Levels (TH Levels).

Level	V_s V	J_b A	V_a V	J_a mA	V_{dc} V	J_{dc} A	V_{nk} V	J_{nk} A	Main flow sccm	Disch. Cath. flow sccm	Neut. Cath. flow sccm	$V_{ck\text{-}cc}$ V
TOC 4	1100	0.71	-150.1	2.71	25.60	6.05	17.37	2.00	8.7	5.21	3.47	6.92
TOC 8	1101	1.10	-180.1	4.84	25.10	8.24	17.40	2.00	15.3	4.02	3.68	6.49
TOC 12	1100	1.49	-180.0	6.75	25.40	10.87	18.50	1.50	21.2	3.28	3.89	5.80
TOC 15	1100	1.76	-180.1	8.30	25.14	13.13	-	-	25.1	2.96	3.60	5.53
TH 4	1100	0.71	-150	1.927	25.61	6.05	16.26	2.0	8.30	2.47	2.40	-
TH 8	1100	1.10	-180	3.139	25.10	8.24	15.32	1.5	14.41	2.47	2.40	-
TH 12	1100	1.49	-180	4.704	25.40	10.87	14.52	1.5	19.86	2.89	2.81	-
TH 15	1100	1.76	-180	5.993	25.14	13.13	14.02	1.5	23.43	3.70	3.60	-

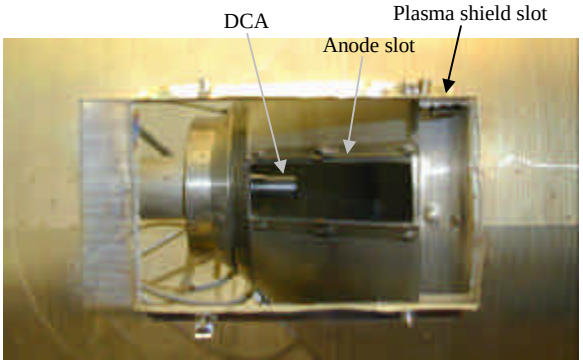

Fig. 1 – Side LIF slots and window mounts with windows removed.

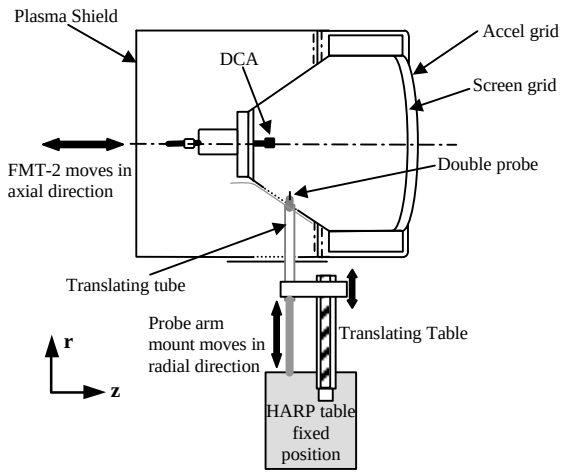

Fig. 2 – FMT-2 orientation w.r.t the HARP for probe insertion, (0, 0) location is 2 mm from the DCA on discharge cathode centerline.

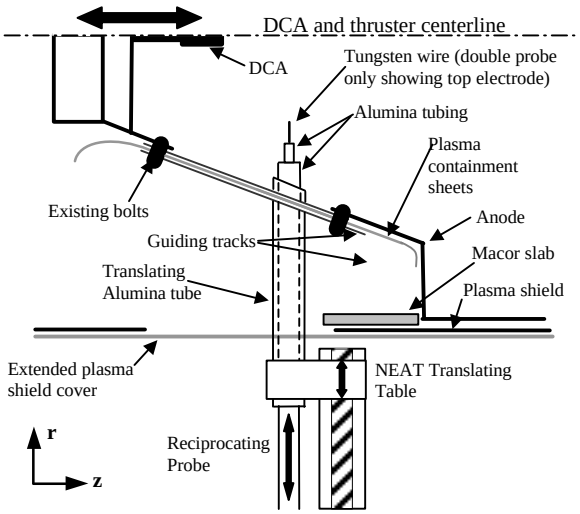

Fig. 3 – Horizontal cross section of the discharge plasma containment mechanism (DPCM).

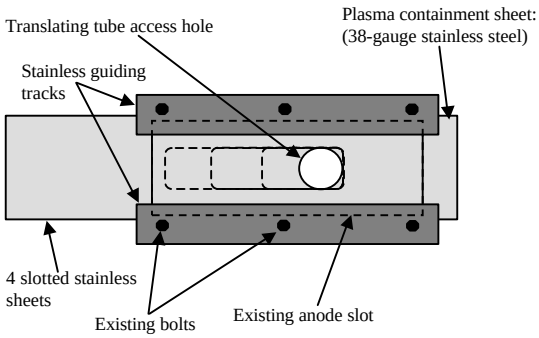

Fig. 4 – Side view schematic of the DPCM hardware covering the anode side slot.

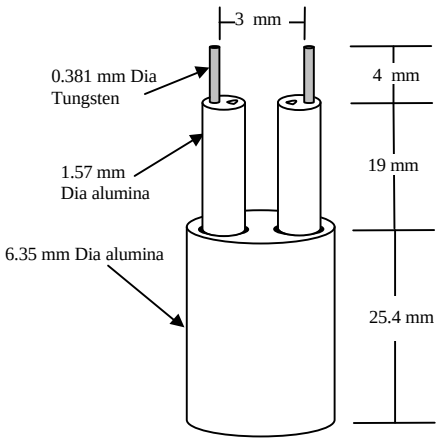

Fig. 5 – Reduced blockage double probe tip design.

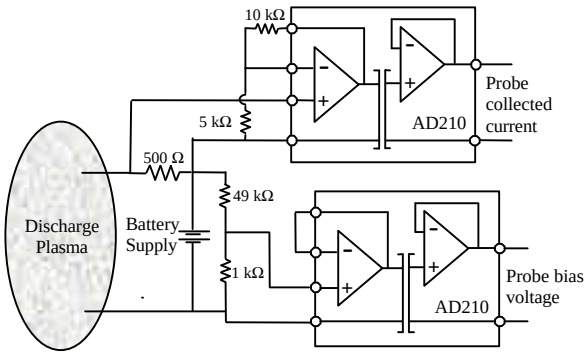

Fig. 6 – Double probe circuit electrical diagram.

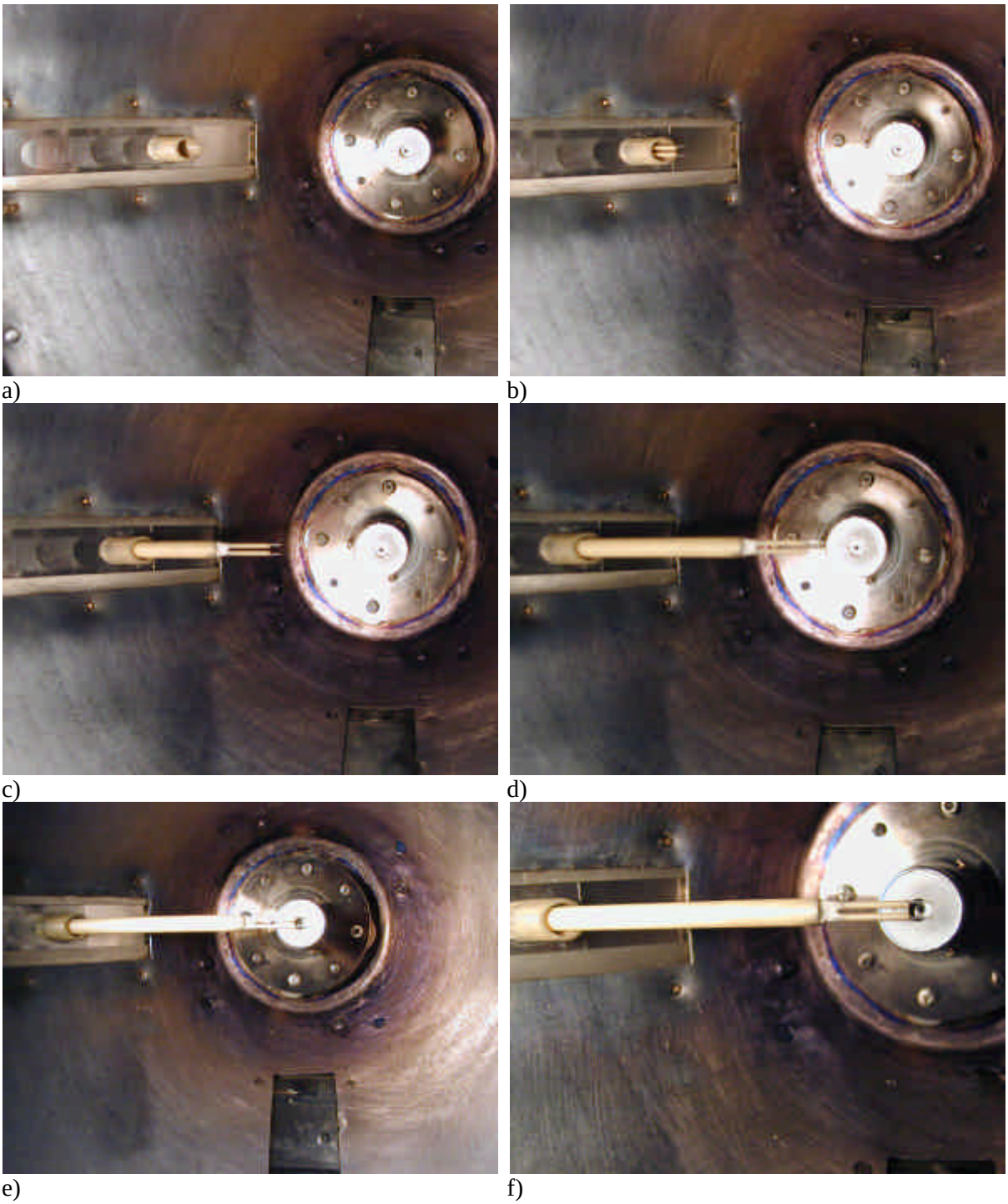

Fig. 7 – Photographs taken inside the discharge chamber prior to engine testing showing the interior of the Discharge Plasma Containment Mechanism (DPCM). Also shown are the double probe and its insertion (a) – (f) at the closest axial location to the Discharge Cathode Assembly (DCA): approximately 2 mm downstream of the DCA.

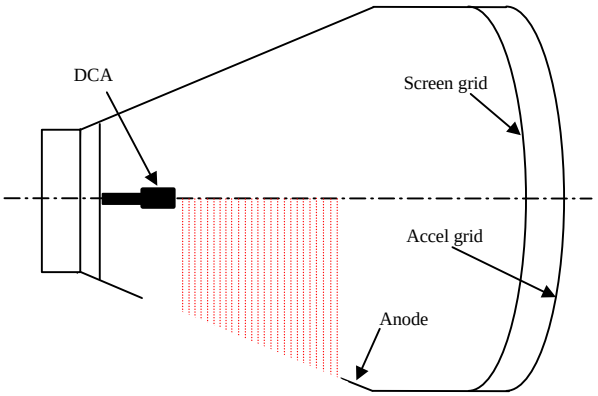

Fig. 8 – Data collection domain. The internal discharge mapping begins 2 mm downstream of the DCA face and extends to 40 mm in 25 steps for an axial resolution of 1.6 mm (1/16 of an inch).

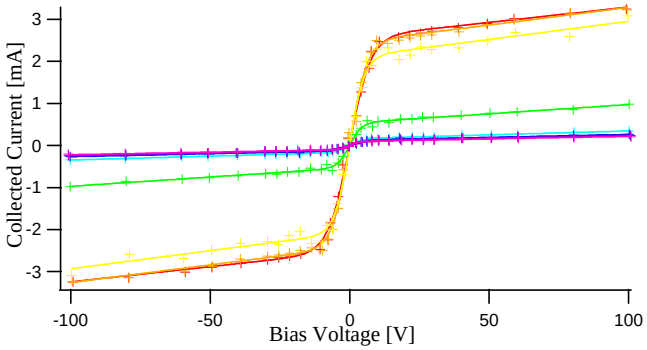

Fig. 9 – Sample of I-V curves (+) and fit curves (-) to raw data for DL 4A. Curves are at axial position 3.6 mm along centerline at the following radial locations: 0 mm (red), 1 mm (orange), 2 mm (yellow), 5 mm (green), 10 mm (light blue), 20 mm (dark blue), 30 mm (purple), 40 mm (light purple).

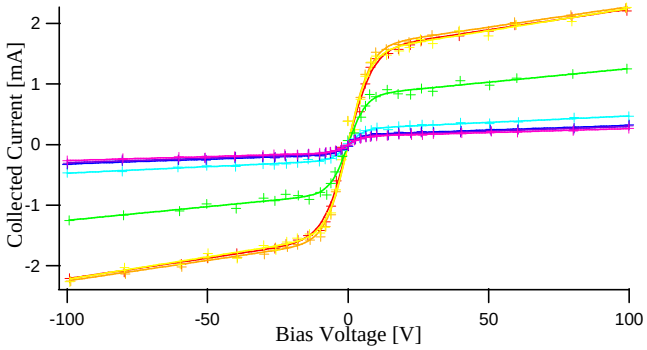

Fig. 10 – Sample of I-V curves (+) and fit curves (-) to raw data for DL 4A. Curves are at axial position 17.9 mm along centerline at the following radial locations: 0 mm (red), 1 mm (orange), 2 mm (yellow), 5 mm (green), 10 mm (light blue), 20 mm (dark blue), 30 mm (purple), 40 mm (light purple).

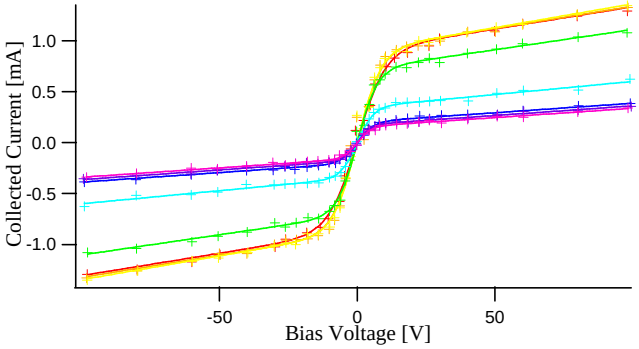

Fig. 11 – Sample of I-V curves (+) and fit curves (-) to raw data for DL 4A. Curves are at axial position 40.1 mm along centerline at the following radial locations: 0 mm (red), 1 mm (orange), 2 mm (yellow), 5 mm (green), 10 mm (light blue), 20 mm (dark blue), 30 mm (purple), 40 mm (light purple).

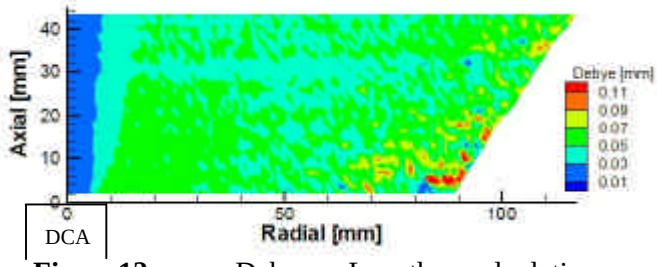

Fig. 12 – Debye Length calculations corresponding to DL 4B: J_{dc} = 6.05 A, V_{dc} = 25.41 V, main flow rate = 19.5 sccm, cathode flow rate = 2.54 sccm (highest magnitude Debye length contour).

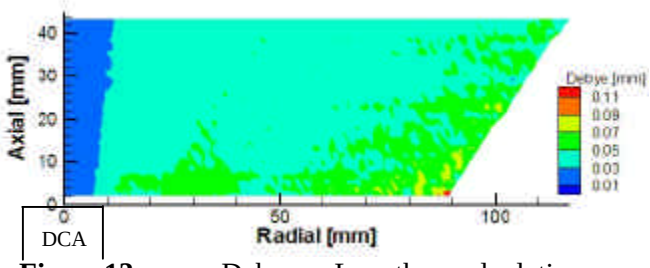

Fig. 13 – Debye Length calculations corresponding to DL 15A: J_{dc} = 13.13 A, V_{dc} = 25.41 V, main flow rate = 11.4 sccm, cathode flow rate = 2.17 sccm (typical Debye length contour).

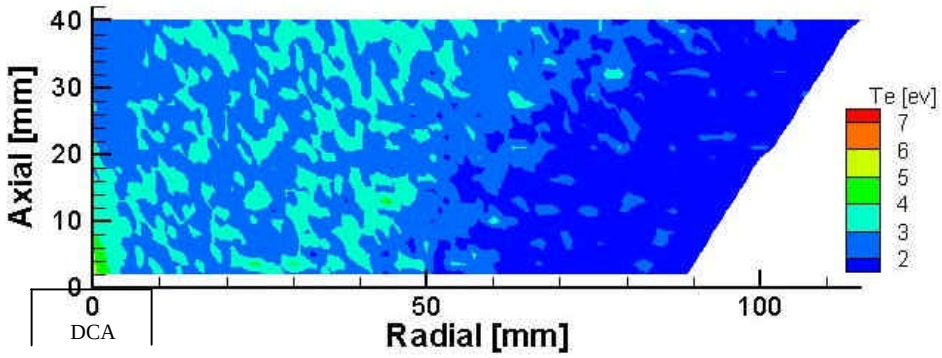

Fig. 14 – Electron Temperature measurements corresponding to TOC 4 (cath. flow = 5.21 sccm).

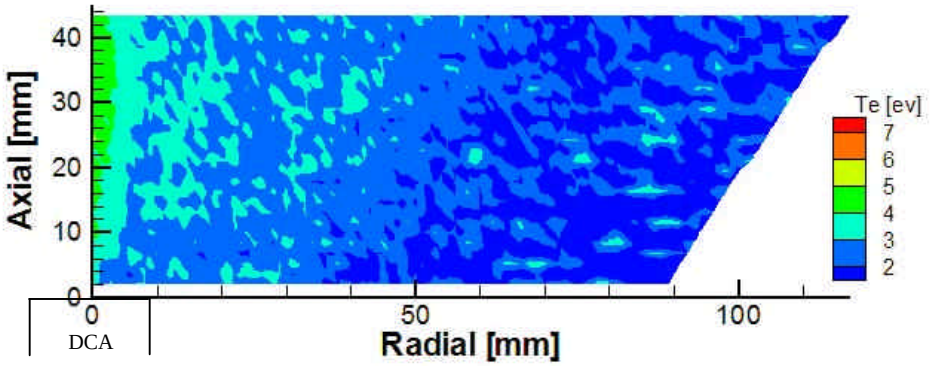

Fig. 15 – Electron Temperature measurements corresponding to DL 4A (cath. flow = 4.07 sccm).

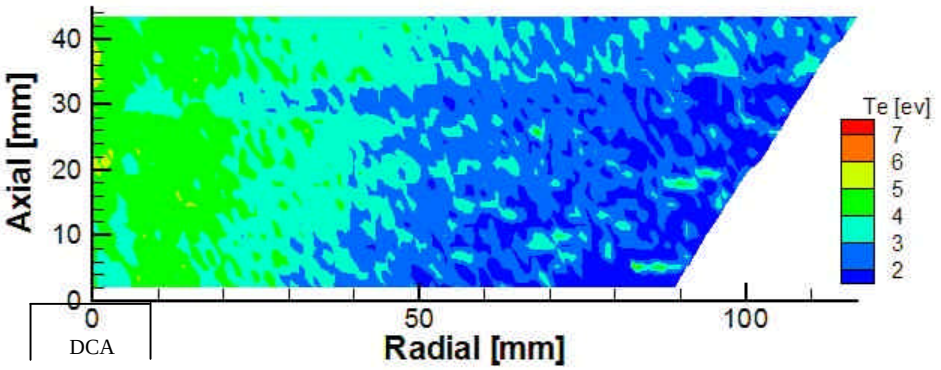

Fig. 16 – Electron Temperature measurements corresponding to DL 4B (cath. flow = 2.54 sccm).

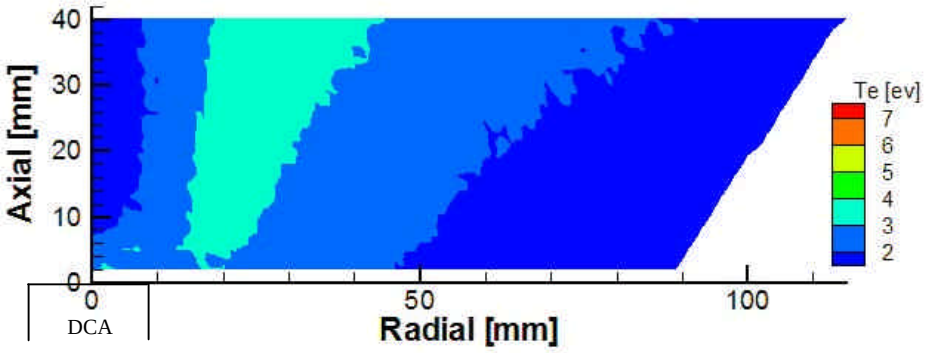

Fig. 17 – Electron Temperature measurements corresponding to Nov02 DL 4 (cath. flow = 2.29 sccm).

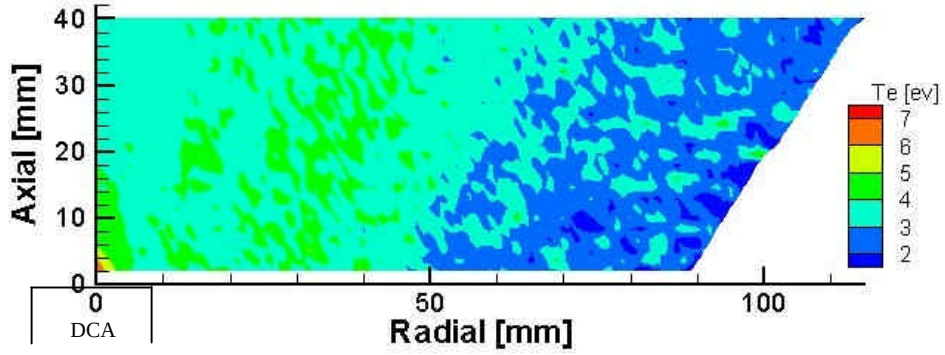

Fig. 18 – Electron Temperature measurements corresponding to TOC 8 (cath. flow = 4.02 sccm).

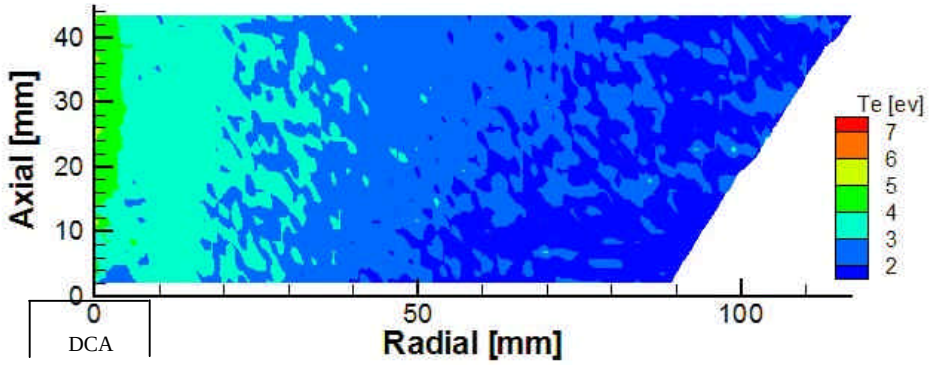

Fig. 19 – Electron Temperature measurements corresponding to DL 8A (cath. flow = 3.37 sccm).

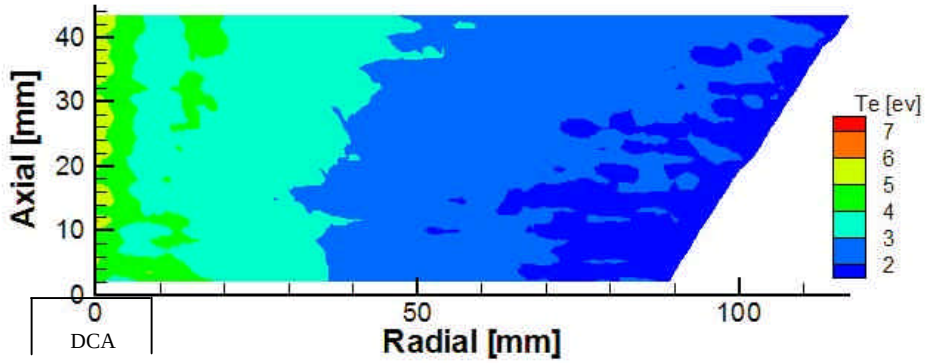

Fig. 20 – Electron Temperature measurements corresponding to DL 8B (cath. flow = 2.54 sccm).

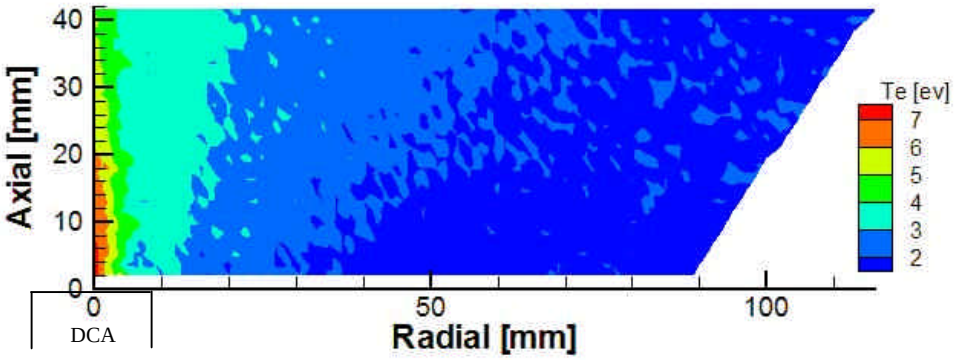

Fig. 21 – Electron Temperature measurements corresponding to DL 8C (cath. flow = 2.78 sccm).

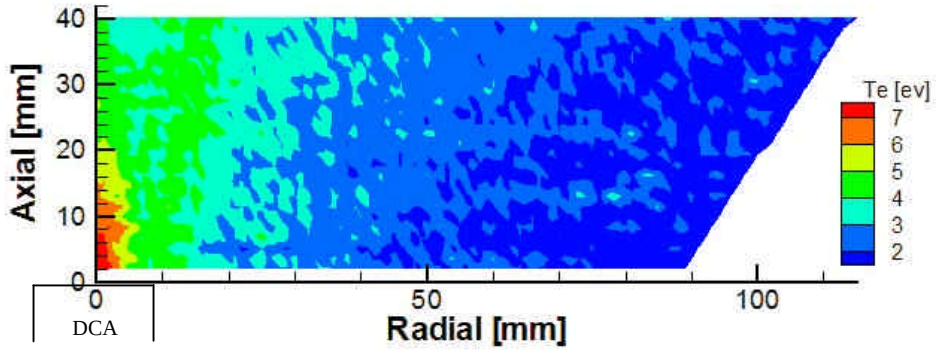

Fig. 22 – Electron Temperature measurements corresponding to DL 8D (cath. flow = 3.17 sccm).

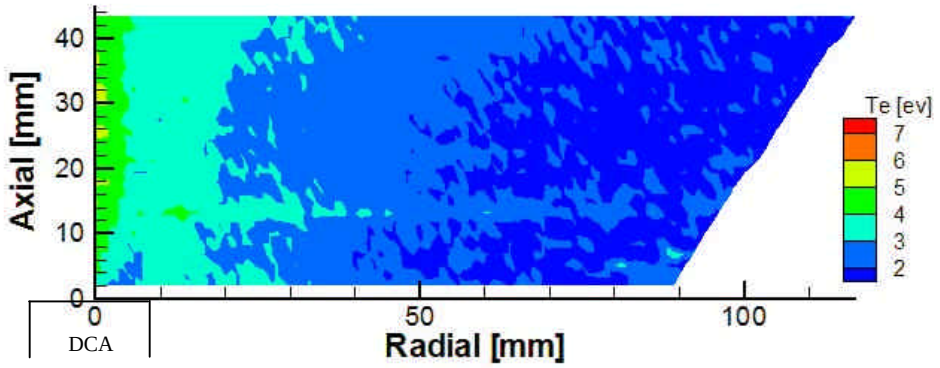

Fig. 23 – Electron Temperature measurements corresponding to DL 12A (cath. flow = 2.23 sccm).

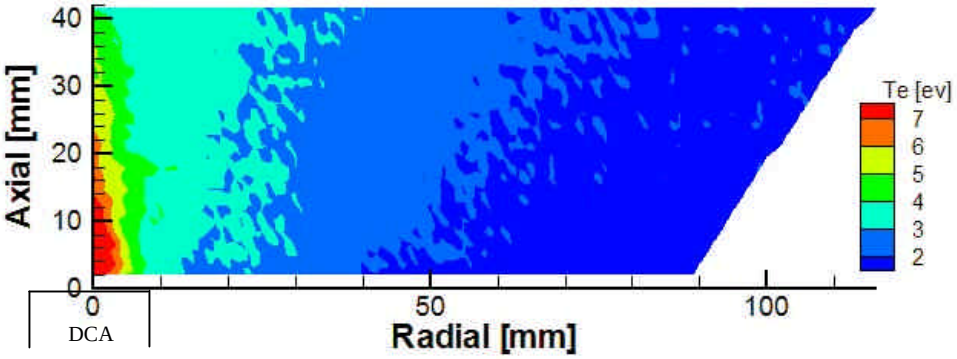

Fig. 24 – Electron Temperature measurements corresponding to DL 12C (cath. flow = 2.89 sccm).

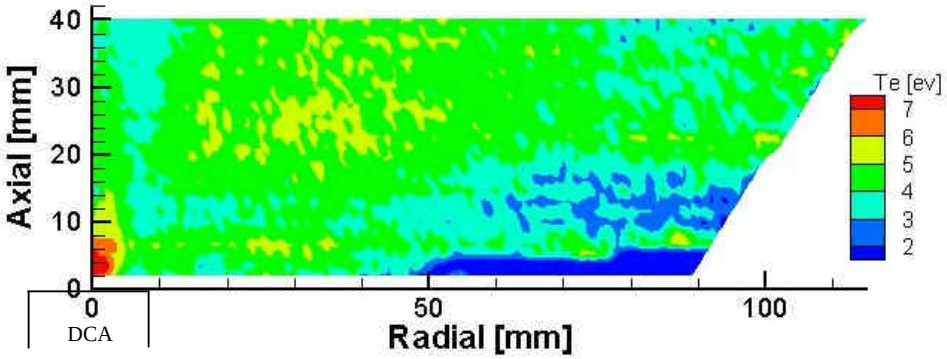

Fig. 25 – Electron Temperature measurements corresponding to TOC 15 (cath. flow = 2.96 sccm).

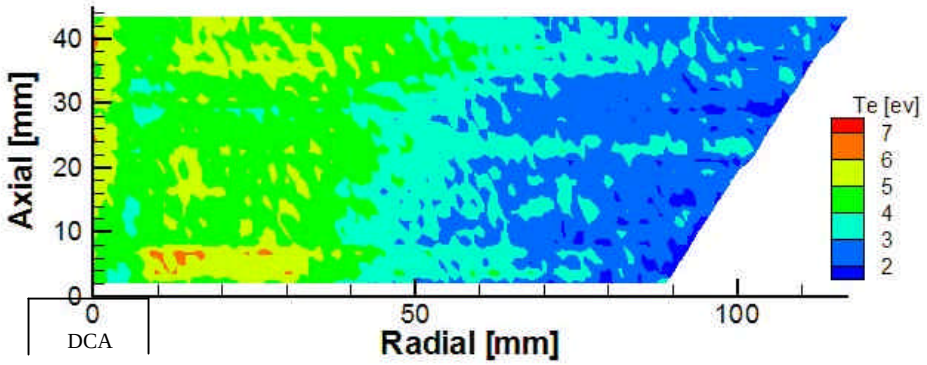

Fig. 26 – Electron Temperature measurements corresponding to DL 15A (cath. flow = 2.17 sccm).

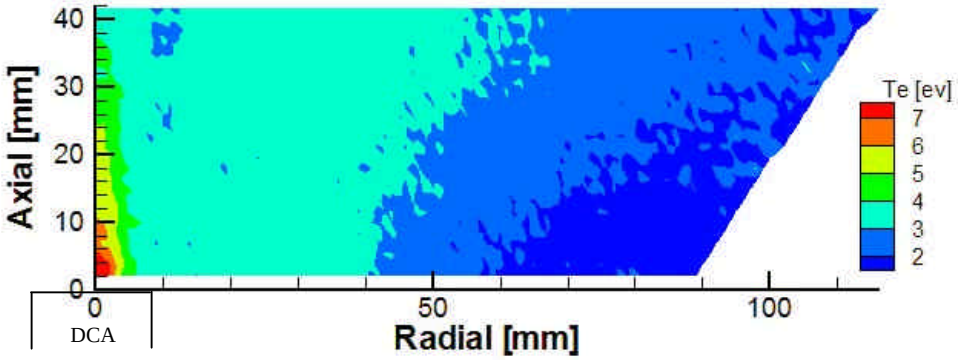

Fig. 27 – Electron Temperature measurements corresponding to DL 15C (cath. flow = 3.47 sccm).

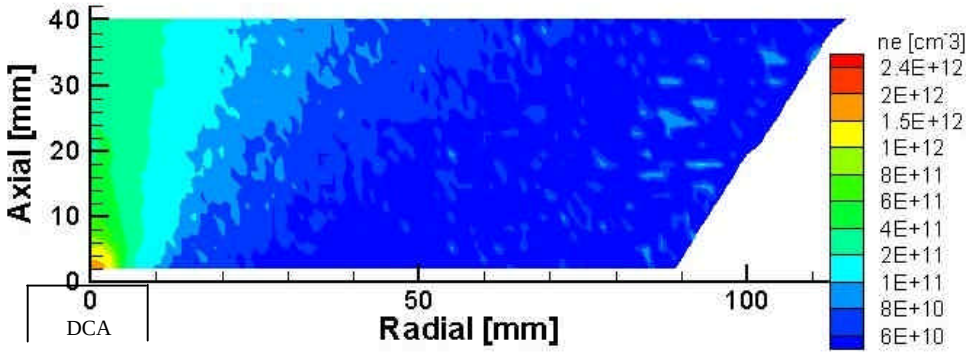

Fig. 28 – Electron number density measurements corresponding to TOC 4 (cath. flow = 5.21 sccm).

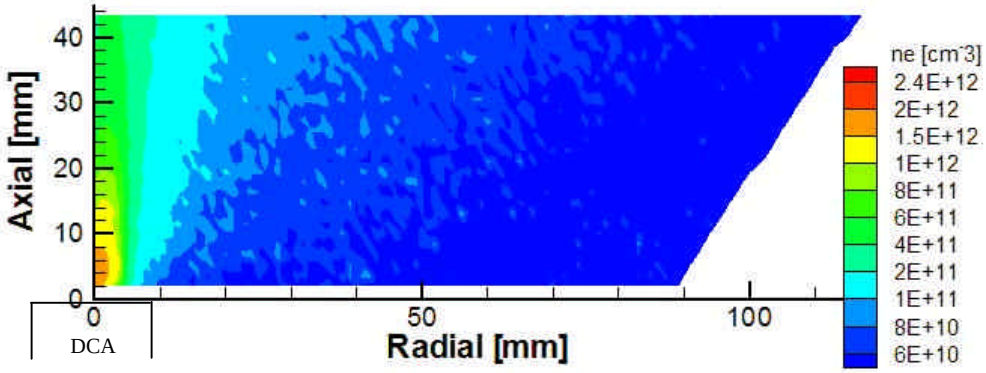

Fig. 29 – Electron number density measurements corresponding to DL 4A (cath. flow = 4.07 sccm).

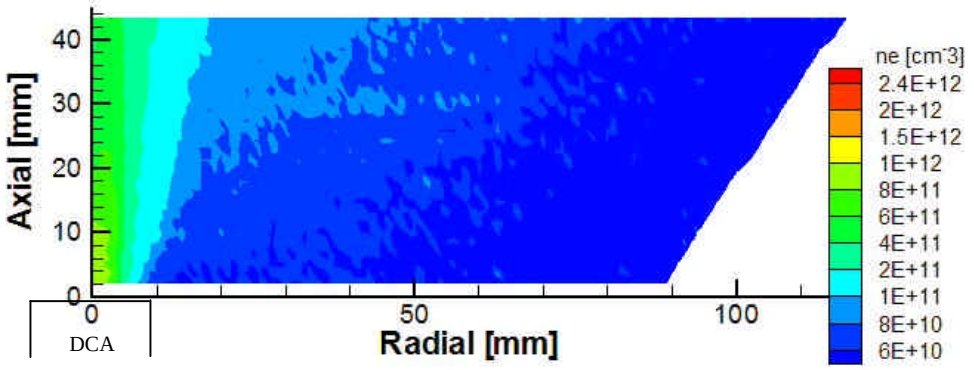

Fig. 30 – Electron number density measurements corresponding to DL 4B (cath. flow = 2.54 sccm).

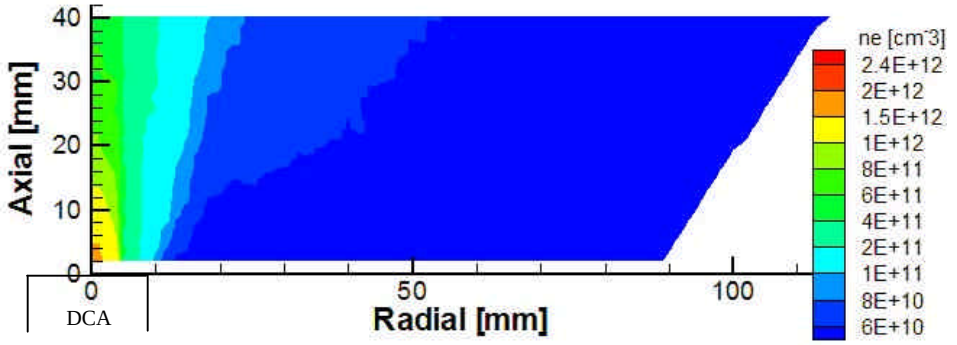

Fig. 31 – Electron number density measurements corresponding to Nov02 DL 4 (cath. flow = 2.29 sccm).

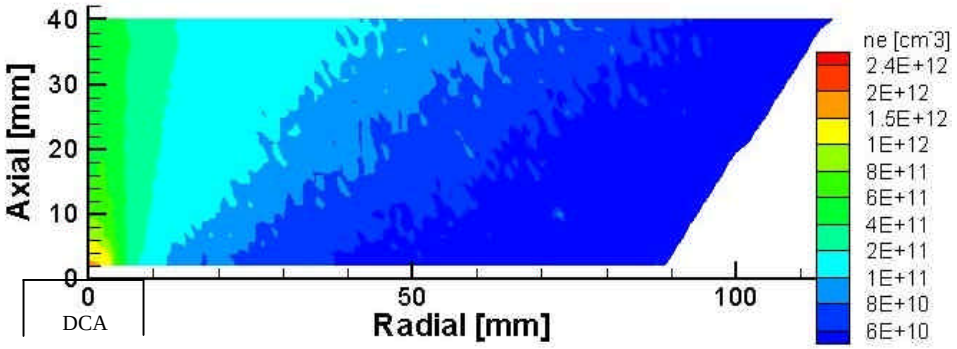

Fig. 32 – Electron number density measurements corresponding to TOC 8 (cath. flow = 4.02 sccm).

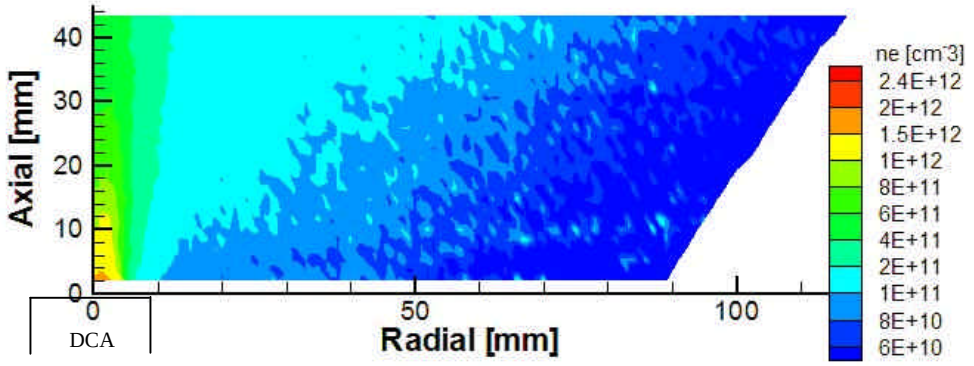

Fig. 33 – Electron number density measurements corresponding to DL 8A (cath. flow = 3.37 sccm).

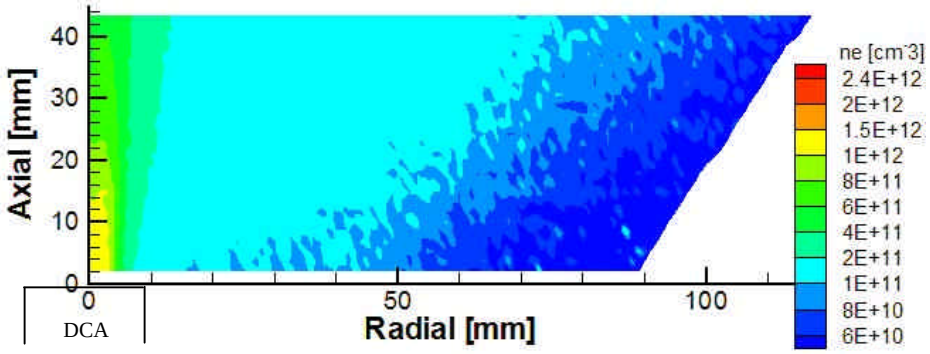

Fig. 34 – Electron number density measurements corresponding to DL 8B (cath. flow = 2.54 sccm).

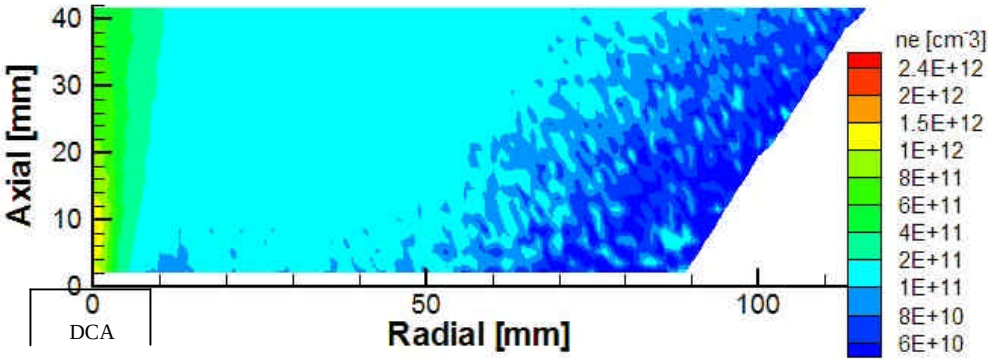

Fig. 35 – Electron number density measurements corresponding to DL 8C (cath. flow = 2.78 sccm).

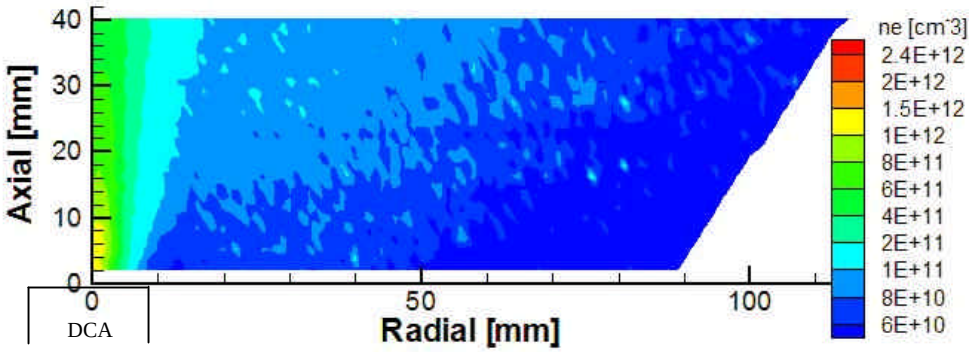

Fig. 36 – Electron number density measurements corresponding to DL 8D (cath. flow = 3.17 sccm).

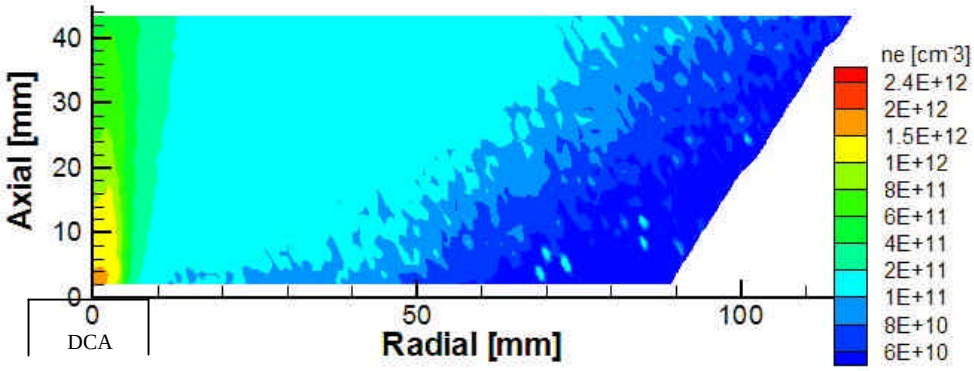

Fig. 37 – Electron number density measurements corresponding to DL 12A (cath. flow = 2.23 sccm).

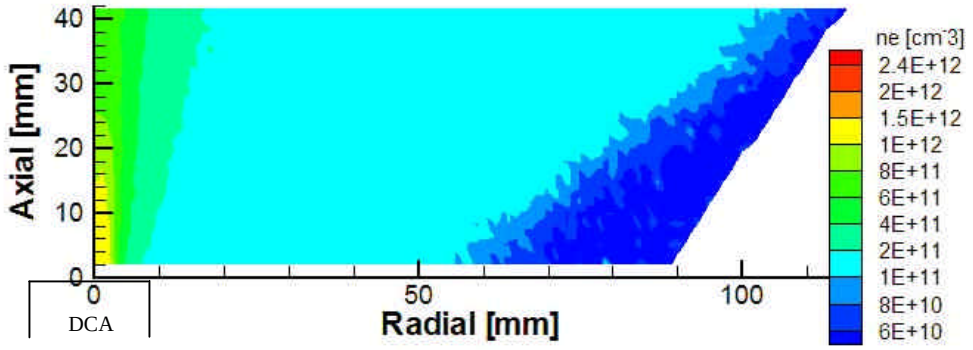

Fig. 38 – Electron number density measurements corresponding to DL 12C (cath. flow = 2.89 sccm).

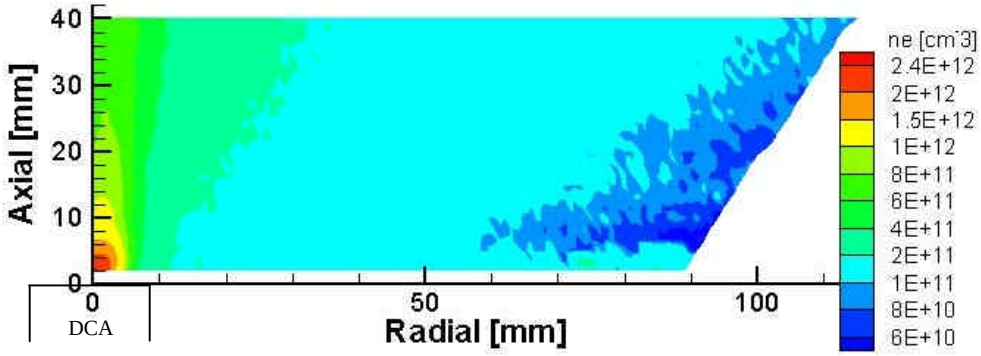

Fig. 39 – Electron number density measurements corresponding to TOC 15 (cath. flow = 2.96 sccm).

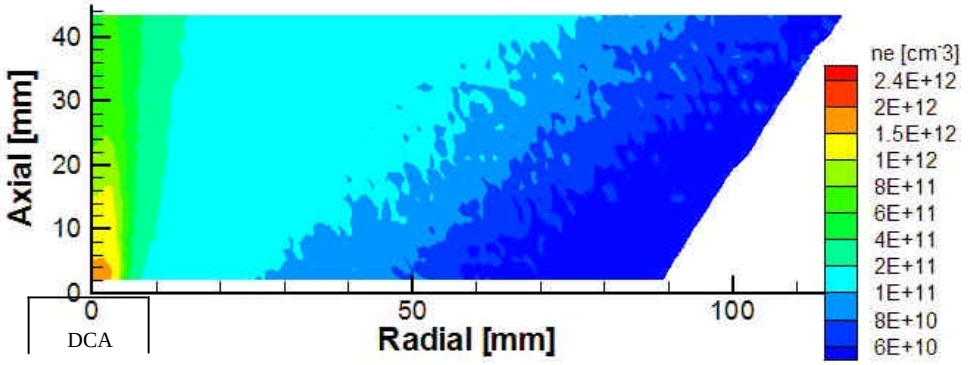

Fig. 40 – Electron number density measurements corresponding to DL 15A (cath. flow = 2.17 sccm).

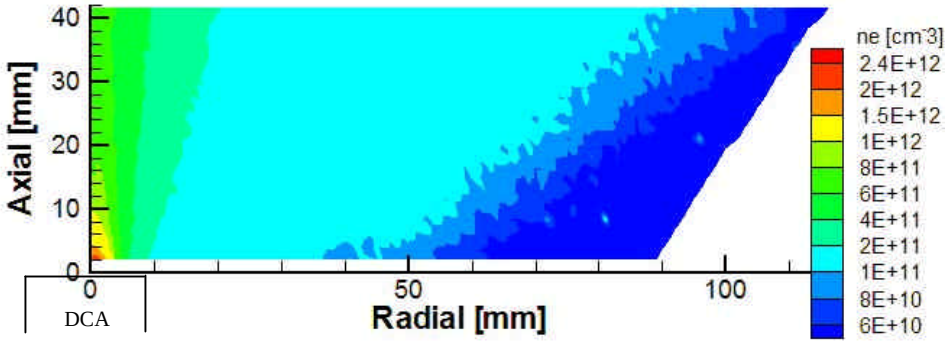

Fig. 41 – Electron number density measurements corresponding to DL 15C (cath. flow = 3.47 sccm).